Journal of Power Sources 214 (2012) 351–357

Contents lists available at SciVerse ScienceDirect

Journal of Power Sources

journal homepage: www.elsevier.com/locate/jpowsour

The influence of Ir and Pt_1Ir_1 structure in metallic multilayers nanoarchitectured electrodes towards ethylene glycol electro-oxidation

R.G. Freitas [a,b], E.P. Antunes [a], P.A. Christensen [b], E.C. Pereira [a,*]

[a] NANOFAEL-LIEC Departamento de Química, Universidade Federal de São Carlos, C.P.: 676, CEP 13565-905, São Carlos, SP, Brazil
[b] School of Chemical Engineering and Advanced Materials, Bedson Building, Newcastle University, Newcastle upon Tyne NE1 7RU, United Kingdom

HIGHLIGHTS

- We studied the electro-oxidation of ethylene glycol at metallic multilayer.
- Metallic multilayer was composed by single and alloy compound into the intralayer.
- Lower activation energy was observed for metallic multilayer.
- We observed CO_2 and CO_L intensity band enhancement for metallic multilayer.

GRAPHICAL ABSTRACT

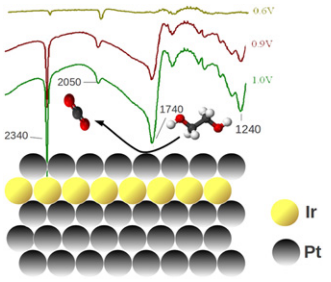

ARTICLE INFO

Article history:
Received 28 March 2012
Received in revised form
25 April 2012
Accepted 29 April 2012
Available online 3 May 2012

Keywords:
Nanostructured electrodes
Electrocatalysis
Metallic multilayer
In situ FTIR

ABSTRACT

This paper presents a study of the electro-oxidation of ethylene glycol (EG) at metallic multilayer electrodes: $Pt_{pc}/Ir_x/Pt_y$ (Pt_{pc} = polycrystalline Pt, x and y denote the number of monolayers of Ir intralayer and Pt outer layer, respectively) and $Pt_{pc}/(Pt_1Ir_1)_x/Pt_y$ (ie a 1:1 alloy of Pt and Ir was employed as intralayer). For comparison, data are also presented for Pt_{pc}. Although Pt and Ir have similar crystallographic structures, the work reported shows for the first time that the electrocatalytic properties of the Pt outer layer are affected significantly by the composition of the intralayer. The voltammetry data show that the $Pt_{pc}/Ir_{3.0}/Pt_{3.0}$ metallic multilayer electrode exhibits a peak current density 78% higher than that observed using Pt_{pc}, in agreement with activation energy measurements on the electro-oxidation of EG which showed: $Pt_{pc}/Ir_{3.0}/Pt_{3.0}$ (26 kJ mol^{-1}) < Pt_{pc} (44 kJ mol^{-1}) < $Pt_{pc}/(Pt_1Ir_1)_{3.0}/Pt_{3.0}$ (46 kJ mol^{-1}). The FTIR experiments showed that the main products for the oxidation of the diol at the electrodes are similar: CO_L, CO_2 and glycolic and/or oxalic acid over Pt_{pc} and $Pt_{pc}/Ir_{3.0}/Pt_{3.0}$ metallic multilayer electrodes. However, significantly more CO_2 and CO_L were observed at $Pt_{pc}/Ir_{3.0}/Pt_{3.0}$ compared to Pt_{pc} electrodes.

1. Introduction

The giant magnetoresistance (GMR) effect was first reported by Fert et al. [1] and Grunberg et al. [2] and is associated with metallic multilayers (MM) with each layer comprising a few monolayers of metal atoms. Although the electronic and magnetic properties of MM have been extensively investigated [3–6], significantly less is known about the electrochemistry of these materials. We have investigated the electrocatalytic properties of MM [7–10] and reported the "Giant Metallic Electrocatalytic effect" (GME) [11]. To our knowledge, we were the first to report the potential application of MM as electrocatalysts for the oxidation of small organic molecules [9], and were able to show that metal multilayers such as Pt_{pc}/Metal/Pt (Metal = Rh, Ru, Bi and Ir), i.e. having a Pt surface layer, exhibited higher catalytic activities than polycrystalline Pt, Pt_{pc}.

* Corresponding author. Tel./fax: +55 16 3351 8214.
E-mail address: ernesto@ufscar.br (E.C. Pereira).

0378-7753/$ – see front matter © 2012 Elsevier B.V. All rights reserved.
doi:10.1016/j.jpowsour.2012.04.099

Thus, the peak current densities observed during the electro-oxidation of methanol, ethanol, formaldehyde and formic acid were increased by ca. 295%, 266%, 140% and 380%, respectively, compared to Pt_{pc}. Also, the onset potential for ethanol oxidation was shifted 100 mV towards more negative values using MM anodes e.g. Pt/Rh/Pt compared to Pt_{pc} [8]. Recently, we have shown that a $Pt_{pc}/Ir_{250}/Pt_{250}$ MM nanostructured electrode was able to oxidise ethanol selectively to CO_2 in acid electrolyte [12].

Novel nanostructured electrocatalysts such as MM electrodes are important as a result of the potential for high activity and selectivity in electrochemical transformations, particularly those relevant to fuel cell technology [13]. Thus, catalysts for the anode of the Direct Methanol Fuel Cell (DMFC) have been extensively researched [14] due to the high energy density of methanol ($11\ kWh\ L^{-1}$) [15] and the possible application of DMFCs as power sources for portable applications. However, methanol is primarily produced from oil and is not readily synthesized from renewable feedstocks [16,17]. In contrast, ethanol is routinely produced on an industrial scale from biomass [18] whilst glycerol is produced as a side product from biodiesel synthesis; ethylene and propylene glycol can be produced in a straightforward process from glycerol and the identification of a high value or high volume use for ethylene glycol could tip biodiesel production firmly into commercial viability [19]. Furthermore, polyhydric alcohols such as ethylene glycol have higher theoretical energy densities than methanol [20,21]. Clearly, the production of polyhydric alcohols as products or byproducts of renewable and sustainable chemical processing of biomass and their subsequent use as fuels in fuel cells is extremely attractive. However, whilst hydrogen electro-oxidation is facile and clean [22], even the electro-oxidation of methanol is beset with problems associated with the chemisorption of this relatively simple organic molecule [23], and the oxidation of any molecules more complicated than methanol incurs a penalty in terms of poor kinetics and selectivity towards the production of CO_2 [24,25].

In situ FTIR spectroscopy has proved an invaluable tool in the study of mechanism at the electrode/electrolyte interface [26,27], particularly with relevance to anode catalysis in fuel cells. Christensen and Hamnet [28] investigated the electrochemical oxidation of ethylene glycol (EG) at Pt_{pc} under both acidic and basic conditions. The products observed were pH dependent: CO_2 and glycolic acid were the primary products in acid; whilst glycolate, oxalate and CO_3^{2-} were the main products in alkaline solution. Vielstich et al. [29] employed *in situ* FTIR spectroscopy to study EG oxidation at several Pt_xRu_y electrodes. The authors observed the onset potential for EG oxidation shifted 200 mV to more negative values compared to that observed at Pt_{pc} due to the promotional effect of Ru. Carbon dioxide, glycolic acid and/or oxalic acid were observed as products, with the selectivity towards CO_2 increasing with Ru content. Other workers have reported studies on EG oxidation using on line and/or *in situ* spectroscopic tools [30–32]. However, to our knowledge there are no studies on EG electro-oxidation over metallic multilayers, particularly using *in situ* FTIR spectroscopy.

In general, on polycrystalline metallic electrodes, individual crystallites expose specific surface structures and consequently active sites to the electrolyte. There is no long-range order and the inter-crystalline areas may show a variety of defects such as grain boundaries, lattice imperfections, inclusions and even oxide layers. Such defects play a major role in electrocatalysis [33,34]. In addition, the factors responsible for significant enhancement of electrocatalytic activity, such as the bifunctional mechanism [35] and electronic effects [36] are not completely understood. We have previously reported [9,10] that the electrocatalytic activity of MM nanostructured electrodes is directly related to the composition and thickness of the intralayer [9,10], and hence a systematic study of MM electrodes as a function of intralayer/surface layer composition using *in situ* FTIR spectroscopy is timely.

Although Pt and Ir have the same crystalline structure, they are different from an electronic point of view. Thus, the aim of the work reported in this paper was to investigate the electrocatalytic activity of MM electrodes having only Ir or a 1:1 PtIr alloy as the intralayer, ie. $Pt_{pc}/Ir/Pt$ or $Pt_{pc}/Pt_1Ir_1/Pt$. Also, different thicknesses of the Ir and Pt_1Ir_1 intralayers and Pt outerlayer were investigated with respect to the oxidation of ethylene glycol in acid solution. The effect of thickness and intralayer composition on ethylene glycol electro-oxidation was studied for both types of MM electrode. Factorial design was employed to determine the minimum number of experiments required to investigate the effect of the preparation variables on the electrocatalytic activity, leading to the best composition and MM electrodes thickness.

2. Experimental

2.1. Electrode preparation

Polycrystalline Pt ($0.64\ cm^2$) substrates were mechanically polished with diamond paste down to 1.0 μm, and washed with acetone and deionised water (Millipore Milli-Q system, 18 MΩ cm). The electrodeposition of the intralayer and outerlayer was carried out as follows: the Ir intralayer was electrodeposited from a solution of 10^{-4} M $IrCl_3 \cdot 3H_2O$ (Sigma–Aldrich, 99.9%) in 0.1 M $HClO_4$ (Sigma–Aldrich, 70%) at a potential of 0.05 V *vs.* reference hydrogen electrode (RHE). The required intralayer thickness (in terms of the number x of monolayers, ML) was achieved on the basis of the charge required. The electrode was then washed with copious amounts of water and transferred to another electrochemical cell containing 10^{-4} M $H_2PtCl_6 \cdot 6H_2O$ (Sigma–Aldrich, ~38%Pt) in 0.1 M $HClO_4$ (Sigma–Aldrich, 70%). The Pt outerlayer was deposited at a potential of 0.05 V *vs.* RHE; again, the thickness of the layer in terms of y ML was determined on the basis of the charge passed. The $Pt_{pc}/Ir_x/Pt_y$ MM nanostructured electrodes so produced were washed with Millipore water.

The MM electrodes employing PtIr alloys as the intralayer, were prepared by electrodeposition from 10^{-4} M $IrCl_3 \cdot 3H_2O + 10^{-4}$ M $H_2PtCl_6 \cdot 6H_2O$ in 0.1 M $HClO_4$ at 0.05 V *vs.* RHE to give PtIr with a 1:1 ratio of Pt to Ir and a thickness of x ML. The subsequent treatment of the electrodes and deposition of the Pt outerlayer was as described above. These electrodes are designated as $Pt_{pc}/(Pt_1Ir_1)_x/Pt_y$ below.

The oxidation of ethylene glycol (Sigma–Aldrich, 99.8%) was investigated in 0.1 M $HClO_4$ and all current densities were normalized to the electroactive surface area calculated from hydrogen desorption [37]. Finally, the activation energies (E_a) for ethylene glycol electro-oxidation over Pt_{pc}, $Pt_{pc}/Ir_{3.0}/Pt_{3.0}$ and $Pt_{pc}/(Pt_1Ir_1)_{3.0}/Pt_{3.0}$ MM anodes were obtained using the Arrhenius equation. The peak current densities for ethylene glycol electro-oxidation were obtained from linear sweep voltammetry over the temperature range from 5 to 35 °C, and employed to calculate the activation energies.

2.2. Electrode characterization

The electrochemical characterization of the MM electrodes was carried out using a potentiostat/galvanostat Autolab PGSTAT 30. Voltammetric curves were measured in 0.1 M $HClO_4$ solution in the potential range between 0.05 and 1.55 V *vs.* RHE. A $2.0\ cm^2$ Pt plate (Sigma–Aldrich, 99.99%) was used as auxiliary electrode. Prior to the experiments, the solutions were sparged with N_2 for 30 min.

In situ FTIR spectra ($4\ cm^{-1}$ resolution, 256 co-added and averaged scans, 40 s per scanset) were collected using a Varian 7000

spectrometer equipped with a liquid nitrogen cooled MCT detector. The spectroelectrochemical cell was home-built and fitted with a hemispherical CaF_2 window (Medway optics Ltd). The cell was vertically mounted on the lid of the sample compartment of the spectrometer and described in detail elsewhere [38–42]. The reflective working electrode was mounted on a Teflon body, and electrical contact was maintained by a screw and push rod arrangement, which also maintained good optical contact between the working electrode and the cell window. The angle of incidence of the IR beam (assuming 0° beam divergence) on the CaF_2 ($n = 1.41$, $k = 0$ [43])/electrolyte interface was 46° (normal incidence at CaF_2/air interface), giving an angle of incidence at the Pt electrode (assuming $n = 1.33$ and approximating k to 0 for water) of 51°. Even allowing for ±6° beam spread, the incidence on the inner side of the CaF_2/electrolyte interface is well below the critical angle, hence precluding any enhancement effects due to total internal reflectance [43]. The optical path-length was estimated from the 1640 cm^{-1} H–O–H scissor band in the single beam reference spectrum, using an extinction coefficient [44] of 21 mol^{-1} dm^3 cm^{-1} and a water concentration of 55.6 M. The path-lengths in the experiments discussed below were ca. 2.0 μm, giving the thin layer thicknesses of ca. 0.6 μm. Only unpolarized light was used.

The reference spectrum (R_0, 256 co-added and averaged scans at 4 cm^{-1} resolution, 40 s per scanset) was collected and a second spectrum taken at the same potential (to check for electrode movement etc), after which spectra (R) were collected at 0.05 V and then every 100 mV up to 1.5 *vs.* RHE. The spectra below are presented as the ratio (R/R_0) *vs.* cm^{-1} and the data manipulation results in spectra in which peaks pointing up, to $+(R/R_0)$, arise from the loss of absorbing species in R with respect to R_0, and peaks pointing down, to $-(R/R_0)$, to the gain of absorbing species.

2.3. Factorial design

Using the factorial design it is possible to decrease the number of experiments required to investigate a particular system [45,46] compared to traditional methodologies. The determination of the minimum number of experiments required, which must be performed in a factorial design, is the combination of all variables at their different values [45]. In a full factorial design, n^k experiments must be performed, where n is the number of variables and k is the number of values of each one of those variables investigated. Therefore, to investigate three variables, each having two different values, only $2^3 = 8$ experiments are needed. The three variables studied were: intralayer composition (Ir or Pt_1Ir_1 alloy), intralayer thickness (1.2 or 3.0 monolayers) and finally outerlayer thickness (1.2 or 3.0 monolayers). The experiments were carried out in duplicate to calculate the experimental error. Table 1 lists the variables and their values.

3. Results and discussion

Fig. 1 shows cyclic voltammogram of the Pt_{pc}, $Pt_{pc}/Ir_{1.2}$, $Pt_{pc}/(Pt_1Ir_1)_{1.2}$ and $Pt_{pc}/Ir_{1.2}/Pt_{1.2}$ anodes in aqueous perchloric acid; the voltammetric response of the Pt_{pc} electrode was in agreement with literature data [47,48]. The onset potentials for hydride adsorption at the $Pt_{pc}/Ir_{1.2}$ and $Pt_{pc}/(Pt_1Ir_1)_{1.2}$ anodes were similar, i.e. 0.05–0.3 V, and the double layer regions also cover the same potential range, i.e. 0.4–0.8 V.

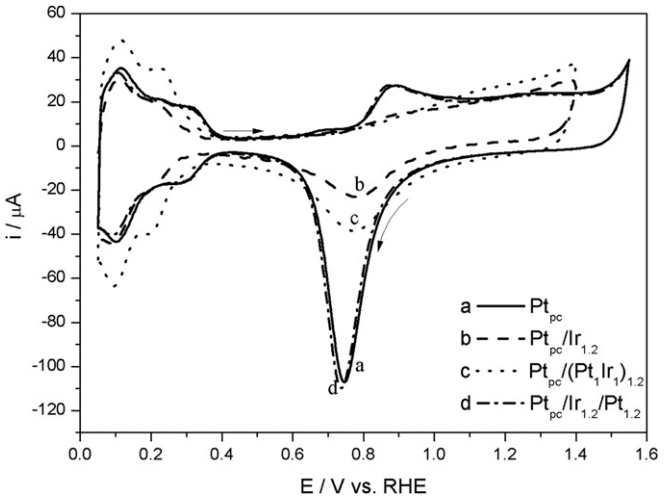

Fig. 1. Cyclic voltammograms obtained for Pt_{pc}, Pt_{pc}/Ir, Pt_{pc}/Pt_1Ir_1 and $Pt_{pc}/Ir/Pt$ metallic multilayer electrodes in 0.1 M $HClO_4$. $\nu = 50$ mV s^{-1}. $T = 25$ °C. See text for details.

As may be seen in Fig. 1, the voltammetric response of the $Pt_{pc}/Ir_{1.2}/Pt_{1.2}$ electrode was similar to Pt_{pc}, suggesting that the $Pt_{pc}/Ir_{1.2}/Pt_{1.2}$ electrode surface is composed only of Pt atoms. In addition, the charge under the hydride features of the $Pt_{pc}/Ir_{1.2}/Pt_{1.2}$ voltammogram was the same as that under the analogous features of the Pt_{pc} voltammogram, showing that the electrochemically active areas of the two electrodes were also identical. In previous papers, the absence of Ru and Rh in the surface layer of Pt_{pc}/Ru/Pt [7] and Pt_{pc}/Rh/Pt [8] MM anodes was confirmed using XPS. The retention of the surface area of the underlying Pt_{pc} was also observed with $Pt_{pc}/(Pt_1Ir_1)_{1.2}/Pt_{1.2}$ electrodes.

Despite the similarity in the crystal structures of Pt and Ir (see below), employing an alloy of these metals as the intralayer in MM electrodes can lead to compressive or tensile strain. Stress relief mechanisms take place when two lattices with different parameters have to coexist, for example, an adsorbate deposited onto a substrate in the case of heteroepitaxy [49]. Due to the reduced number of chemical bonds, surface atoms experience a reduction in electronic density, and hence the lattice tends to contract itself in order to move surface atoms closer together. According to Goyhenex et al. [50], the lattice mismatch between surface and bulk ("surface mismatch") can reach values as large as −2.8% for (111) oriented surfaces, and depends mainly on the ratio between the repulsive and attractive part of the interatomic potential. As discussed by Goyhenex et al. [50], the electronic properties (eg. the energy of the *d*-band centre) of the metal layers in MM electrodes may be affected by surface mismatch. Platinum and iridium are adjacent to each other in the periodic table and exhibit almost the same crystallographic structure. These two elements have space group Fm-3m, cubic closed-packed structures with $\alpha = \beta = \gamma = 90°$; however, $a = b = c = 392.42$ pm and 383.9 pm for Pt and Ir, respectively. Although their crystallographic structures are very similar, the presence of these elements can lead to different surface mismatch values when electrodeposited to form $Pt_{pc}/Ir_x/Pt_y$ and $Pt_{pc}/(Pt_1Ir_1)_x/Pt_y$ metallic multilayers. This change in the structural properties can result in significant enhancement of the electronic properties of the surface layer and hence of electrocatalytic activity,

Table 1
Preparation variables to study the metallic multilayers nanostructured electrodes over ethylene glycol oxidation.

	Levels	
Variables	−	+
Intralayer composition	Ir	Pt_1Ir_1
ML_{In}	1.2	3.0
ML_{Out}	1.2	3.0

and it is this possibility, specifically with respect to EG electro-oxidation, that is evaluated in this paper.

For clarity, of the eight anodes prepared according to factorial design (see Table 1) only the linear sweep voltammograms (LSVs) of the MM electrodes exhibiting highest and lowest peak current densities for EG electro-oxidation (i.e. $Pt_{pc}/Ir_{3.0}/Pt_{3.0}$ and $Pt_{pc}/(Pt_1Ir_1)_{3.0}/Pt_{3.0}$, respectively) are shown in Fig. 2. The data obtained using the polycrystalline Pt electrode are also shown, for comparison.

The voltammetric response of Pt_{pc} in acidic solution containing EG is well known [20,28] and exhibits a peak at 0.86 V and shoulder near 1.5 V see Fig. 2. However, as may be seen from the figure, there is an additional shoulder around 0.65–0.77 V in the LSVs of the MM electrodes, which is absent from the voltammetric response of the Pt_{pc} anode. The process(es) giving rise to this shoulder are unclear, and further work is underway to elucidate this. Roy et al. [51] have observed this shoulder during experiments on the electro-oxidation of methanol at RuO_2 film electrodes on which were dispersed Pt nanoparticles. According to the authors, this feature may be attributed to the dehydrogenation of methanol. Behm et al. [52] had observed similar voltammetric responses in their studies of EG electro-oxidation at Pt nanoparticles using DEMS. According to the authors, the process observed during the positive-going scan corresponds to the oxidation of CO_{ads} to CO_2, and a similar shoulder was also observed and attributed to glycol aldehyde.

From Fig. 2 it may be seen that the $Pt_{pc}/Ir_{3.0}/Pt_{3.0}$ electrode showed a peak current 78% higher than that observed using the Pt_{pc} electrode. The changes in the peak current density and the presence of the pre-peak observed using the MM anodes compared to Pt_{pc} are clear evidence for differences in the mechanistic and/or electronic properties of $Pt_{pc}/Ir_{3.0}/Pt_{3.0}$ and $Pt_{pc}/(Pt_1Ir_1)_{3.0}/Pt_{3.0}$ compared to Pt_{pc}. As was stated above, there is no evidence that the interlayer is exposed to electrolyte, hence the differences evident in the LSVs in Fig. 2 cannot be due to direct involvement of Ir in surface processes, ie. via the bifunctional mechanism [35].

Koper et al. [53] employed periodic DFT-GGA methods to study the interaction of adsorbed CO and OH with a range of substrates, including: Pt_{ML}/Pt, Pt_{ML}/Pt_2Ru, $Pt_{ML}/PtRu_2$ and Pt_{ML}/Ru (0001). The authors observed that the system with the lowest CO binding energy was $Pt_{ML}/Ru(0001)$. This result is in agreement with the data presented in Fig. 2 since the $Pt_{pc}/Ir_{3.0}/Pt_{3.0}$ electrode gives a higher peak current density than the $Pt_{pc}/(Pt_1Ir_1)_{3.0}/Pt_{3.0}$ electrode, and hence suggests a lower CO binding energy on the former electrode. The lower binding energy of CO on these surfaces may be understood in terms of a decrease in the energy of the Pt *d*-band caused by strain in the overlayer, as Pt has to form a (1×1) commensurate monolayer on the intralayer with a lower lattice constant. Mavrikakis et al. [54] investigated the adsorption of O and O_2, and the dissociation of O_2, on a monolayer of Pt covering the (111) facets of Pt_3Co and Pt_3Fe alloys also using the DFT-GGA approach. The authors [54] were able to show that compressive strain tends to decrease the energy of the centre of the *d*-band (ε_d) of transition metals, causing adsorbates to bind less strongly, whereas tensile strain has the opposite effect. The position of ε_d for Pt monolayers also depends both on the strain (geometric effects) and on the electronic interaction between the Pt monolayer and the underlying metal (ligand effect). It has been suggested [55] that the chemical properties of metal monolayers deposited on metallic substrates may be interpreted in terms of a model in which charge transfer between the monolayer and substrate, or changes in the density of states of the monolayer [55] near the Fermi level, lead to shifts of the core levels of the monolayer. Thus, it is not unreasonable to postulate that the Ir in the intralayer can induce compressive strain, which is reflected in the higher peak current density for EG electro-oxidation compared to (Pt_1Ir_1) intralayers. Hence, surface mismatch between monolayers and overlayers play a key role in the electrocatalytic reactions.

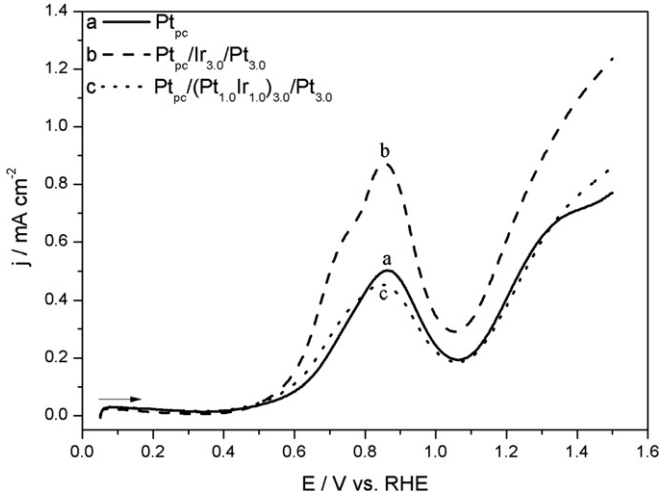

Fig. 2. Linear sweep voltammograms obtained for the electro-oxidation of 0.5 M $C_2H_6O_2$ in 0.1 M $HClO_4$ over Pt_{pc}, $Pt_{pc}/(Pt_1Ir_1)_{3.0}/Pt_{3.0}$ and $Pt_{pc}/Ir_{3.0}/Pt_{3.0}$ metallic multilayer electrodes. $\nu = 50$ mV s^{-1}. $T = 25$ °C.

Thin films have, in general, only one exposed surface, and thus surface energy and its anisotropy are major influences on chemical reactivity [56]. Multilayer systems, in turn, have additional contributions to the surface free energy due to the bonding of the different constituent materials. Thus, chemical reactivity depends on the density of interfaces (number of interface per multilayer thickness) and can reach very high values in nanostructured systems e.g. metallic multilayers electrodes [57]. Hence Rosato et al. [58,59] developed the TB-SMA (tight binding-second moment approximation) method, which is simple enough to derive analytical expressions related to the elastic behaviour of such systems, to describe fully the different stress relief mechanisms, such as stress-driven alloy formation [60], the formation of substrate misfit dislocations [61,62], adsorbate misfit dislocations [63], pseudomorphy [63], pseudoepitaxy [60] and reconstruction [64] slabs systems. Hence, it was decided to investigate whether the electrocatalytic behaviour of metallic multilayers, such as $Pt_{pc}/Ir_{3.0}/Pt_{3.0}$ and $Pt_{pc}/(Pt_1Ir_1)_{3.0}/Pt_{3.0}$ could also be explained in terms of stress relief mechanisms [50].

Using slab geometry and second moment approximation, Treglia et al. [65] formulated that the surface energy can be calculated as:

$$\gamma = \frac{1}{2A}(E(N) - NE_b) \tag{1}$$

where N is the number of atoms in the slab unit cell, A the surface area, $E(N)$ the total energy of the slab, and E_b the energy of the bulk atoms (i.e. the opposite of cohesive energy). The surface stress is a symmetric tensor with elements:

$$\sigma_{ij} = \frac{1}{A}\frac{\partial(A\gamma)}{\partial\varepsilon_{ij}} \tag{2}$$

where ε_{ij} is the strain tensor and $i, j = x, y, z$. Note that a positive (negative) value of σ means a tensile (compressive) surface stress. After full energy relaxation, all the $\sigma_{i,j}$ component are zero. The development of this equation leads to:

$$\sigma_{i,j} = \gamma\delta_{i,j} + \frac{\partial\delta}{\partial\varepsilon_{i,j}}, \quad i,j = x,y \tag{3}$$

Therefore, there are two contributions to the surface stress, the first one is the surface energy and the second one is its strain derivative [65].

Goyhenex et al. [50] calculated using so-called second moment approximation surface mismatches values for Ir and Pt surfaces. The individually values were −1.07 and −2.53% for Ir and Pt (111) oriented surfaces, respectively [50,66]. The larger surface mismatch for Pt compared to Ir can be related to the higher *d*-band filling of Pt. According to the authors [50], the more filled the *nd*-band, the weaker the nuclear charge experienced by the $(n+1)$s electrons, inducing a spatial extension of the electronic density associated to the $(n+1)$s electrons. This effect is observed as an increase in the range of the repulsive part of the interatomic potential when moving from left to right of the periodic table e.g. from Ir to Pt.

As discussed above, Pt and Ir exhibit different values for the surface mismatch. Even for the same intra and outerlayer thickness, the composition of the intralayer (Ir or Pt_1Ir_1 alloy) clearly has a significant influence on the electrocatalytic behaviour of MM electrodes, as observed on Fig. 2. Thus, factorial design was an important tool in assessing the importance of the composition and thickness of layers.

The presentation of the responses using a 2^3 factorial design can be analysed using the cube representation (Fig. 3). The figure shows eight responses (peak current density) at the corner of a cube in which the axes represent the different variables investigated, i.e. the number of interlayers (1.2 or 3.0 ML), number of outerlayers (1.2 or 3.0 ML) and intralayer composition (Ir or Pt_1Ir_1) (Table 1).

As was stated above, the electrode with the highest peak current density was the $Pt_{pc}/Ir_{3.0}/Pt_{3.0}$ electrode. Using the factorial design approach, it was possible to ascertain that the electrocatalytic behaviour was enhanced when using Ir as the intralayer and not Pt_1Ir_1 alloy. In order to analyse the relationship between intralayer composition and layer thickness in more depth, the main effects (intralayer composition, number of intralayers and number of outerlayers), and associated errors were calculated and are shown in Table 2. The most significant parameter was intralayer composition (-0.205 ± 0.045); and its negative value indicating that, on increasing the Ir to Pt_1Ir_1 intralayers level, the peak current density decreased. Therefore, the highest electrocatalytic activity was observed for $Pt_{pc}/Ir_{3.0}/Pt_{3.0}$ MM electrodes, as observed in Fig. 2.

Fig. 4 shows Arrhenius plots of the peak current densities observed at 0.85 V in the linear sweep voltammogram of the most active ($Pt_{pc}/Ir_{3.0}/Pt_{3.0}$), least active ($Pt_{pc}/(Pt_1Ir_1)_{3.0}/Pt_{3.0}$) and Pt_{pc} electrodes as a function of temperature between 5 and 35 °C.

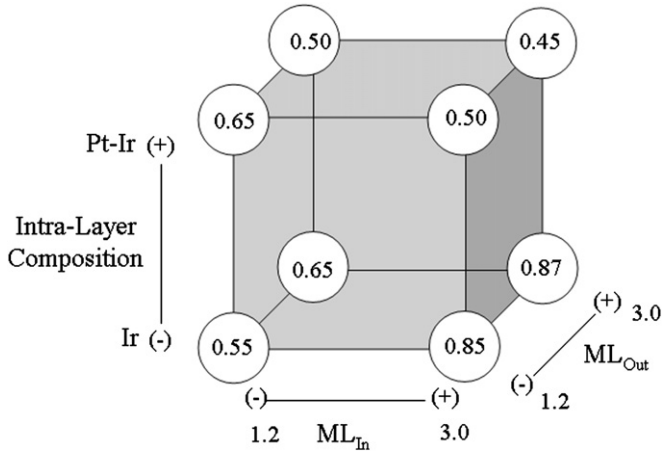

Fig. 3. Factorial design cube showing the results of eight values of current peak density regarding the variables of each level.

Table 2
Mean values of current peak density, main effects and interaction calculation between two and three effects.

Medium	0.628 ± 0.023 (mA cm^{-2})
Main Effects	
1. (Intralayer composition)	−0.205 ± 0.045
2. (ML_{In})	0.08 ± 0.045
3. (ML_{Out})	−0.02 ± 0.045

The activation energies were found to be 26, 44 and 46 kJ mol^{-1}, respectively for the $Pt_{pc}/Ir_{3.0}/Pt_{3.0}$, Pt_{pc} and $Pt_{pc}/(Pt_1Ir_1)_{3.0}/Pt_{3.0}$ MM electrodes. Iwasita et al. [67] prepared 85:15 and 50:50 Pt:Ru alloys using UHV techniques, and observed activation energies for methanol electro-oxidation around 60 kJ mol^{-1}. Behm et al. [68] studied ethanol electro-oxidation at a carbon-supported Pt catalyst at elevated temperature and pressure, and the activation energy for complete conversion to CO_2 was typically c.a. 76 kJ mol^{-1}. As observed above, the marked lower activation energy for $Pt_{pc}/Ir_{3.0}/Pt_{3.0}$ MM electrodes (26 kJ mol^{-1}) reflects the key role of the Ir layer beneath the Pt outerlayer. Although Ir and Pt exhibit the same crystalline structure as previously discussed, it is possible to modulate electronic effects, which lead to an enhancement in electrocatalysis activity.

The complete cleavage of C–C bond is difficult to observe under electrochemical conditions [24] and it is the limiting factor in the development of ethanol fuel cells. From electronic structure calculations (DFT), it was shown that the lowest energy transition states for C–O and C–C bond cleavage for ethanol on e.g. $Pt_3Sn(111)$ involve the formation of adsorbed 1-hydroxyethylidene (CH_3COH) and acetyl (CH_3CO) species, respectively [69] which were confirmed experimentally by *in situ* FTIR reflectance data [70,71] and differential electrochemical mass measurements [72–74]. Hence *in situ* FTIR was employed to study the electro-oxidation of EG at the most active MM electrode ($Pt_{pc}/Ir_{3.0}/Pt_{3.0}$) and, for comparison, at Pt_{pc}.

Fig. 5a and b shows *in situ* FTIR spectra obtained during the oxidation of 0.5 M EG in 0.1 M $HClO_4$ at the Pt_{pc} and $Pt_{pc}/Ir_{3.0}/Pt_{3.0}$ electrodes. These spectra were recorded during an experiment in which the potential was stepped in 100 mV increments from 0.05 V to 1.5 V, and normalised to the reference spectrum collected at

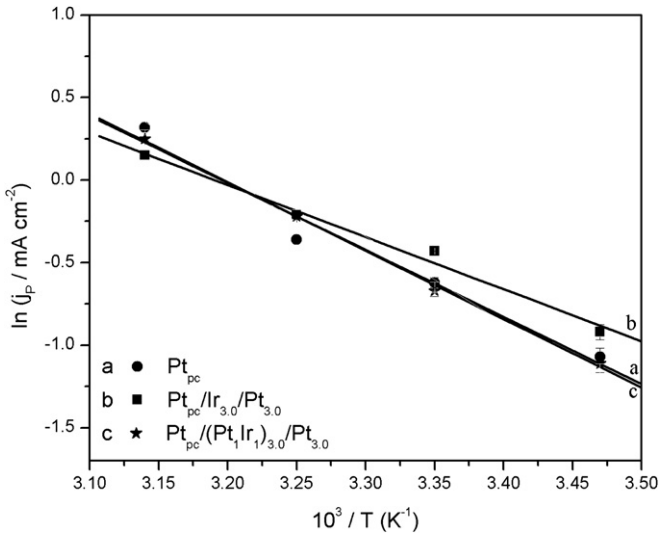

Fig. 4. Arrhenius plots of the peak current observed at 0.85 V in the linear sweep voltammogram of 0.5 M $C_2H_6O_2$ in 0.1 M $HClO_4$ at Pt_{pc}, $Pt_{pc}/(Pt_1Ir_1)_{3.0}/Pt_{3.0}$ and $Pt_{pc}/Ir_{3.0}/Pt_{3.0}$ anodes as a function of temperature. Other conditions as in Fig. 2.

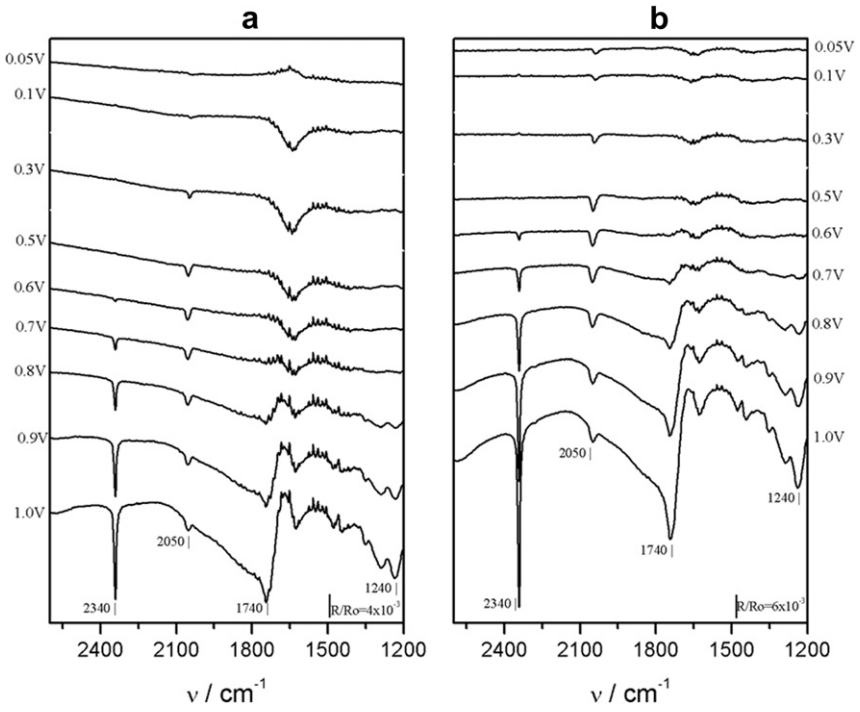

Fig. 5. *In situ* FTIR spectra (4 cm^{-1} resolution, 256 co-added and averaged scans, 40 s per scanset) collected from a) Pt_{pc} and b) $Pt_{pc}/Ir_{3.0}/Pt_{3.0}$ metallic multilayer electrodes during potential step experiments from 0.05 V. Electrolyte: 0.5 M $C_2H_6O_2$ in 0.1 M $HClO_4$. Potential as indicated. Reference spectra were collected at 0.05 V.

0.05 V. However, for clarity, only the spectra collected up to 1.0 V are shown.

A band at 2340 cm^{-1} may be seen in Fig. 5a and b corresponding to CO_2 formation [28,29]. Bands at 1740 cm^{-1} and 1280 cm^{-1} appear in the spectra of both electrodes and correspond to the C═O and the C—O stretches of the carboxylic acid groups of glycolic and/or oxalic acid [28,29].

Fig. 6 shows plots of the integrated band intensities of the CO_L and CO_2 features in Fig. 5. As may be seen from Fig. 6, there is a ca. 180% increase in the maximum intensity of the CO_L feature observed using $Pt_{pc}/Ir_{3.0}/Pt_{3.0}$ compared to Pt_{pc} electrode, as well as a ca. 55% increase in the CO_2 band intensity observed at 1.5 V. It is interesting to note that the former corresponds to the potential of the shoulder in the linear sweep voltammogram in Fig. 2, and this is under further investigation.

From Fig. 6 it is clear that the onset of CO_2 production corresponds to the maximum in the CO_L intensities, suggesting that CO_L is the intermediate in the production of CO_2 as expected on the basis of the indirect path mechanism [28,29,52].

As stated above, the band at 1280 cm^{-1} corresponds to the C—O stretching of a carboxylic acid group, which may be attributed to glycolic and/or oxalic acid. Thus, the selectivity of the Pt_{pc} and MM electrodes may be estimated by a consideration of the ratio of the CO_2 and 1280 cm^{-1} bands (I_{CO_2}/I_{1280}) as a function of electrode potential, and the relevant plots are shown in Fig. 7.

The higher selectivity of the $Pt_{pc}/Ir_{3.0}/Pt_{3.0}$ electrode towards C—C bond cleavage is clear from the figure. The maximum ratio for

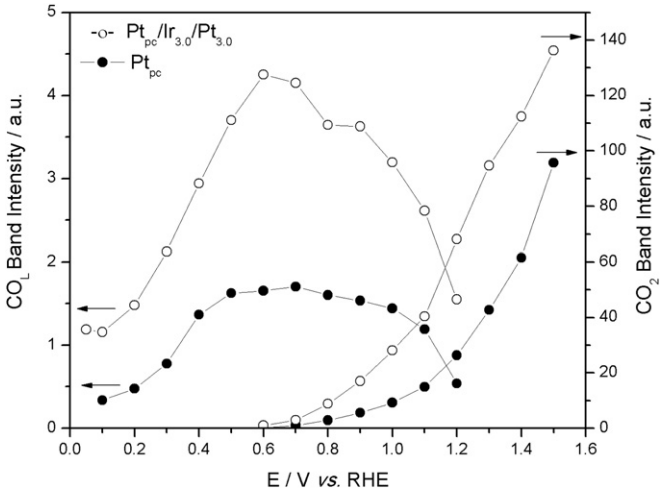

Fig. 6. Plots of the intensities of the CO_L and CO_2 bands in Fig. 5(a) and (b) as function of potential.

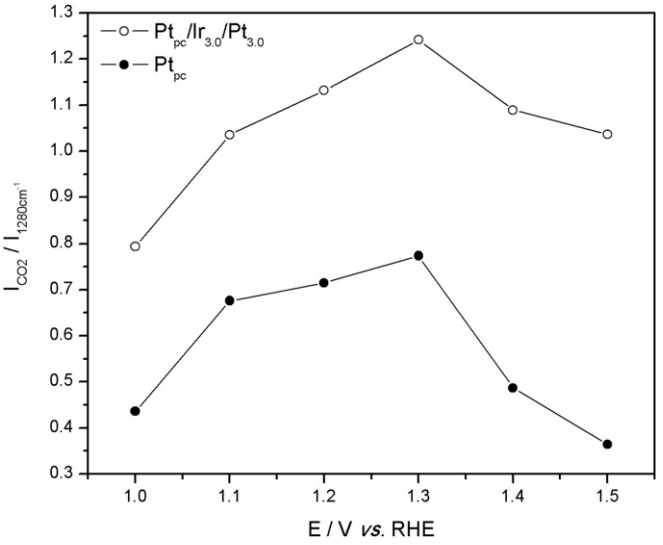

Fig. 7. Plots of the intensities of the CO_2 bands in Fig. 5(a) and (b) normalized to the 1280 cm^{-1} (C—O stretch) bands as function of potential.

both electrodes occurred at 1.3 V, at which potential the I_{CO_2}/I_{1280} ratio is 65% higher for $Pt_{pc}/Ir_{3.0}/Pt_{3.0}$ than Pt_{pc}.

4. Conclusions

The results of this work show that, although Pt and Ir exhibit similar crystallographic structures, the $Pt_{pc}/Ir_{3.0}/Pt_{3.0}$ MM electrode shows the highest electrocatalytic activity and selectivity for EG oxidation compared to Pt_{pc} and $Pt_{pc}/(Pt_1Ir_1)_{3.0}/Pt_{3.0}$. Room temperature LSV and *in situ* FTIR experiments were supported by the activation energy data for EG electro-oxidation at the three electrodes which showed 26 kJ mol^{-1} at $Pt_{pc}/Ir_{3.0}/Pt_{3.0}$ compared to 44 kJ mol^{-1} at Pt_{pc} and 46 kJ mol^{-1} at $Pt_{pc}/(Pt_1Ir_1)_{3.0}/Pt_{3.0}$. The results were interpreted in terms of a model of surface mismatch in which the change in the structural properties resulting from replacing Ir in the intralayer by (Pt_1Ir_1) alloy results in a significant enhancement of the electronic properties of the Pt surface layer and hence of electrocatalytic activity. This is caused by the lower surface mismatch induced by Ir compared to Pt, which leads to compressive strain, causing adsorbates to bind less strongly.

Acknowledgements

The authors thank the Brazilian Research Funding Institutions CNPq, CAPES and FAPESP (10/05555-2 and 03/09933-8), and the School of Chemical Engineering and Advanced Materials, Newcastle University for financial support.

References

[1] M.N. Baibich, J.M. Broto, A. Fert, F.N.V. Dau, F. Petroff, Phys. Rev. Lett. 61 (1988) 21.
[2] G. Bisnach, P. Grunberg, F. Saurenbach, W. Zinn, Phys. Rev. B 39 (1989) 7.
[3] I. Bakonyi, L. Peter, Prog. Mater. Sci. 55 (2010) 107.
[4] S.Y. Chen, Y.D. Yao, J.M. Wu, J. Magn. Magn. Mater. 310 (2007) 1914.
[5] S.B. Sakrani, Y.B. Wahab, Y.C. Lau, J. Alloys Comp. 434 (2007) 598.
[6] D.K. Pandya, P. Gupta, S.C. Kashyap, S. Chaudhary, J. Magn. Magn. Mater. 321 (2009) 974.
[7] S.G. Lemos, R.T.S. Oliveira, M.C. Santos, P.A.P. Nascente, L.O.S. Bulhoes, E.C. Pereira, J. Power Sources 163 (2007) 695.
[8] R.T.S. Oliveira, M.C. Santos, B.G. Marcussi, P.A.P. Nascente, L.O.S. Bulhoes, E.C. Pereira, J. Electroanal. Chem. 575 (2005) 177.
[9] R.T.S. Oliveira, M.C. Santos, L.O.S. Bulhoes, E.C. Pereira, J. Electroanal. Chem. 569 (2004) 233.
[10] R.G. Freitas, E.P. Antunes, E.C. Pereira, Electrochim. Acta 54 (2009) 1999.
[11] R.G. Freitas, E.C. Pereira, Electrochim. Acta 55 (2010) 7622.
[12] R.G. Freitas, E.C. Pereira, P.A. Christensen, Electrochem. Commun. 13 (2011) 1147.
[13] V.R. Stamenkovic, B.S. Mun, M. Arenz, K.J.J. Mayrhofer, C.A. Lucas, G. Wang, P.N. Ross, M.N. Markovic, Nature Mater. 6 (2007) 241.
[14] S. Basri, S.K. Kamarudim, W.R.W. Daud, Z. Yaakub, Int. J. Hydrogen Energy 35 (2010) 7957.
[15] D.N. Prater, J.J. Rusek, Appl. Energy 74 (2003) 135.
[16] H. Li, H. Hong, H. Jin, R. Cai, Appl. Energy 87 (2010) 2846.
[17] T. Ren, M.K. Patel, Resour. Conserv. Recycl. 53 (2009) 513.
[18] J.R. Mielenz, Curr. Opin. Microbiol. 4 (2001) 324.
[19] J. Janaun, N. Ellis, Renew. Sust. Energy Rev. 14 (2010) 1312.
[20] V. Selvaraj, M. Vinoba, M. Alagar, J. Colloid Interface Sci. 322 (2008) 537.
[21] M.C. Halseid, Z. Jusys, R.J. Behm, J. Electroanal. Chem. 644 (2010) 103.
[22] F. Alcaide, G. Alvarez, P.L. Cabot, O. Miguel, A. Querejeta, Int. J. Hydrogen Energy 35 (2010) 11634.
[23] T. Iwasita, Electrochim. Acta 47 (2002) 3663.
[24] G.A. Camara, T. Iwasita, J. Electroanal. Chem. 578 (2005) 315.
[25] G.A. Camara, R.B. de Lima, T. Iwasita, J. Electroanal. Chem. 585 (2005) 128.
[26] P.A. Christensen, in: J. Yarwood, R. Douthwaite, S. Duckett (Eds.), Spectroscopic Properties of Inorganic and Organometallic Compounds, RSC Publishing, London, 2010, p. 125.
[27] P.A. Christensen, in: P.R. Unwin (Ed.), Encyclopaedia of Electrochemistry – Instrumentation in Electroanalytical Chemistry, Wiley-VCH, Weinheim, 2003, p. 530.
[28] P.A. Christensen, A. Hamnett, J. Electroanal. Chem. 260 (1989) 1101.
[29] R.B. de Lima, V. Paganin, T. Iwasita, W. Vielstich, Electrochim. Acta 49 (2003) 85.
[30] A. Dailey, J. Shin, C. Korzeniewski, Electrochim. Acta 44 (1989) 1147.
[31] L. Demarconnay, S. Brimaud, C. Coutanceau, J.M. Leger, J. Electroanal. Chem. 601 (2007) 169.
[32] Y.F. Fan, Z.Y. Zhou, C.H. Zhen, C.J. Fan, S.G. Sun, Electrochim. Acta 49 (2004) 4659.
[33] S.G. Sun, P.A. Christensen, A. Wieckowski, in: , In situ Spectroscopic Studies of Adsorption at the Electrode and Electrocatalysis, vol. 15, Elsevier, 2007, p. 471.
[34] G. Wang, T. Takeguchi, E.N. Muhamad, T. Yamanaka, W. Ueda, Int. J. Hydrogen Energy 36 (2011) 3322.
[35] M. Watanabe, S. Motoo, J. Electroanal. Chem. 60 (1975) 267.
[36] P. Liu, J.K. Norskov, Fuel Cells 1 (2001) 192.
[37] S. Trassati, O.A. Petrii, Pure Appl. Chem. 63 (1991) 719.
[38] W.F. Lin, P.A. Christensen, A. Hamnett, M.S. Zei, G. Ertl, J. Phys. Chem. B 104 (2000) 6642.
[39] W.F. Lin, P.A. Christensen, A. Hamnett, J. Phys. Chem. B 104 (2000) 12002.
[40] W.F. Lin, P.A. Christensen, J.M. Jin, A. Hamnett, in: S.G. Sun, P.A. Christensen, A. Wieckowski (Eds.), In-situ Spectroscopic Studies of Adsorption at the Electrode and Electrocatalysis, Elsevier, Amsterdam, 2007, p. 99.
[41] J.M. Jin, W.F. Lin, P.A. Christensen, J. Electroanal. Chem. 563 (2004) 71.
[42] P.A. Christensen, J.M. Jin, W.F. Lin, A. Hamnett, J. Phys. Chem. B 108 (2004) 3391.
[43] P.W. Faguy, W.R. Fawcett, Appl. Spectrosc. 44 (1990) 1309.
[44] J.G. Bayly, V.B. Kartha, W.H. Stevens, Infrared Phys. 3 (1963) 211.
[45] G.E.P. Box, W.G. Hunter, J.S. Hunter, Statistic for Experiments – An Introduction to Design, Data Analysis and Model Building, John Wiley & Sons, New York, 1978, 306.
[46] B.B. Neto, I.S. Scarminio, R.E. Bruns, Como Fazer Experimentos, Editora Unicamp, Campinas, 2001.
[47] B.E. Conway, Prog. Surf. Sci. 49 (1995) 331.
[48] H. Kose, M. Bicer, C. Tutunoglu, A.O. Aydın, I. Sisman, Electrochim. Acta 54 (2009) 1680.
[49] H. Ibach, Surf. Sci. Rep. 29 (1997) 193.
[50] H. Bulou, C. Goyhenex, Appl. Surf. Sci. 188 (2002) 163.
[51] L.X. Yan, R.G. Allen, K. Scott, P.A. Christensen, S. Roy, Electrochim. Acta 50 (2005) 1217.
[52] H. Wang, Z. Jusys, R.J. Behm, Electrochim. Acta 54 (2009) 6484.
[53] T.E. Shubina, M.T.M. Koper, Electrochim. Acta 47 (2002) 3621.
[54] Y. Xu, A.V. Ruban, M. Mavrikakis, J. Am. Chem. Soc. 126 (2004) 4717.
[55] A. Ruban, B. Hammer, P. Stoltze, H.L. Skriver, J.K. Norskov, J. Mol. Catal. Lett. A: Chem. 115 (1997) 421.
[56] V. Vovok, G. Schmitz, A. Hutten, S. Heitmann, Acta Mater. 55 (2007) 3033.
[57] C.V. Tompson, Scr. Metal Mater. 28 (1993) 167.
[58] V. Rosato, M. Guillope, B. Legrand, Phil. Magn. 59 (1989) 321.
[59] F. Cleri, V. Rosato, Phys. Rev. B 48 (1993) 22.
[60] C. Goyhenex, H. Bulou, J.P. Deville, G. Treglia, Phys. Rev. B 60 (1999) 2781.
[61] I. Meunier, G. Treglia, J.M. Gay, B. Aufray, B. Legrand, Phys. Rev. B 59 (1999) 10910.
[62] I. Meunier, G. Treglia, B. Legrand, R. Tetot, B. Aufray, J.M. Gay, Appl. Surf. Sci. 162 (2000) 219.
[63] C. Goyhenex, G. Treglia, Surf. Sci. 446 (2000) 272.
[64] M. Guilope, B. Legrand, Surf. Sci. 215 (1989) 577.
[65] S. Olivier, A. Saul, G. Treglia, Appl. Surf. Sci. 212 (2003) 866.
[66] I. Meunier, PhD Thesis, Marseille, France, 2001.
[67] E.A. Batista, H. Hoster, T. Iwasita, J. Electroanal. Chem. 554 (2003) 265.
[68] S. Sun, M.C. Halseid, M. Heinen, Z. Jusys, R.J. Behm, J. Power Sources 190 (2009) 2.
[69] R. Alcala, J.W. Shabaker, G.W. Huber, M.A. Sanchez-Castillo, J.A. Dumesic, J. Phys. Chem. B 109 (2005) 2074.
[70] F. Vigier, C. Coutanceau, F. Hahn, E.M. Belgsir, C. Lamy, J. Electroanal. Chem. 563 (2004) 81.
[71] S.H. Xia, H.D. Liess, T. Iwasita, J. Electroanal. Chem. 437 (1997) 233.
[72] H. Wang, Z. Jusys, R.J. Behm, J. Power Sources 154 (2006) 351.
[73] M.G. Pereira, M.D. Jiménez, M.P. Elizalde, A.M. Robledo, N.A. Vante, Electrochim. Acta 49 (2004) 3917.
[74] N. Fujiwara, K.A. Friedrich, U. Stimming, J. Electroanal. Chem. 472 (1999) 120.